This is a repository copy of *JWST/NIRSpec observations of brown dwarfs in the Orion Nebula Cluster*.

White Rose Research Online URL for this paper:
https://eprints.whiterose.ac.uk/219213/

Version: Published Version

eprints@whiterose.ac.uk
https://eprints.whiterose.ac.uk/

JWST/NIRSpec Observations of Brown Dwarfs in the Orion Nebula Cluster

K. L. Luhman[1,2] , C. Alves de Oliveira[3] , I. Baraffe[4,5] , G. Chabrier[4,5] , E. Manjavacas[6,7] , R. J. Parker[8,10] , and P. Tremblin[9]

[1] Department of Astronomy and Astrophysics, The Pennsylvania State University, University Park, PA 16802, USA; kll207@psu.edu
[2] Center for Exoplanets and Habitable Worlds, The Pennsylvania State University, University Park, PA 16802, USA
[3] European Space Agency, European Space Astronomy Centre, Camino Bajo del Castillo s/n, 28692 Villanueva de la Cañada, Madrid, Spain
[4] Physics & Astronomy Department, University of Exeter, Exeter, EX4 4QL, UK
[5] Ecole Normale Supérieure de Lyon, CRAL, CNRS UMR 5574, 69364, Lyon Cedex 07, France
[6] AURA for the European Space Agency, Space Telescope Science Institute, 3700 San Martin Drive, Baltimore, MD 21218, USA
[7] Department of Physics & Astronomy, Johns Hopkins University, Baltimore, MD 21218, USA
[8] Department of Physics and Astronomy, The University of Sheffield, Hicks Building, Hounsfield Road, Sheffield S3 7RH, UK
[9] Université Paris-Saclay, UVSQ, CNRS, CEA, Maison de la Simulation, 91191, Gif-sur-Yvette, France

Abstract

We have used the multiobject mode of the Near-Infrared Spectrograph (NIRSpec) on board the James Webb Space Telescope (JWST) to obtain low-resolution 1–5 μm spectra of 22 brown dwarf candidates in the Orion Nebula Cluster, which were selected with archival images from the Hubble Space Telescope. One of the targets was previously classified as a Herbig–Haro (HH) object and exhibits strong emission in H I, H_2, and the fundamental band of CO, further demonstrating that HH objects can have bright emission in that CO band. The remaining targets have late spectral types (M6.5 to early L) and are young based on gravity-sensitive features, as expected for low-mass members of the cluster. According to theoretical evolutionary models, these objects should have masses that range from the hydrogen burning limit to 0.003–0.007 $M_\odot$. Two of the NIRSpec targets were identified as proplyds in earlier analysis of Hubble images. They have spectral types of M6.5 and M7.5, making them two of the coolest and least massive known proplyds. Another brown dwarf shows absorption bands at 3–5 μm from ices containing H_2O, CO_2, OCN^-, and CO, indicating that it is either an edge-on class II system or a class I protostar. It is the coolest and least massive object that has detections of these ice features. In addition, it appears to be the first candidate for a protostellar brown dwarf that has spectroscopy confirming its late spectral type.

Unified Astronomy Thesaurus concepts: Brown dwarfs (185); L dwarfs (894); Star forming regions (1565); Initial mass function (796); James Webb Space Telescope (2291); Circumstellar disks (235); Protoplanetary disks (1300); Proplyds (1296); Protostars (1302)

Materials only available in the online version of record: data behind figure

1. Introduction

The Orion Nebula Cluster (ONC, A. A. Muench et al. 2008; C. R. O'Dell et al. 2008) is one of the most attractive sites for studying the formation of brown dwarfs. Because of the youth (1–5 Myr, R. D. Jeffries et al. 2011) and proximity (390 ± 2 pc, J. Maíz Apellániz et al. 2022) of the ONC, its substellar members can be detected down to very low masses. The richness of the cluster (∼2000 members) allows good statistical constraints on the mass function and other properties of its brown dwarfs (e.g., binary fraction, disk fraction). The high stellar density and resulting compactness on the sky of the ONC make it amenable to deep imaging and multiobject spectroscopy to identify and characterize the substellar members. In addition, the ONC can be compared to sparser star-forming regions to search for variations with stellar density in the mass function of brown dwarfs, and perhaps the occurrence rate of ejected giant planets (K. W. Smith & I. A. Bonnell 2001; J. R. Hurley & M. M. Shara 2002; F. Flammini Dotti et al. 2019; E. C. Daffern-Powell et al.

2022). The primary challenge in observing brown dwarfs in the ONC is the bright emission from the Orion Nebula, which reduces the sensitivity of images and spectroscopy. UV radiation from the most massive O star in the ONC, θ^1 C Ori, is ultimately responsible for most of that emission through the generation of an H II region and the heating of the surrounding molecular cloud. The UV photons and the H II region do offer a distinct advantage in studying the members of the ONC, making it possible for high-resolution imaging to spatially resolve ionization fronts surrounding circumstellar disks (known as "proplyds") and the silhouettes of disks against the background nebular emission. Many examples of these disks were discovered by the Hubble Space Telescope (HST) in its early years of operation (C. R. O'Dell et al. 1993; C. R. O'Dell & Z. Wen 1994; M. J. McCaughrean & C. R. O'Dell 1996; C. R. O'Dell & S. K. Wong 1996; J. Bally et al. 2000; L. Ricci et al. 2008).

Surveys for brown dwarfs in the ONC have detected several hundred candidates using optical and near-infrared imaging with ground-based telescopes (M. J. McCaughrean & J. R. Stauffer 1994; M. Simon et al. 1999; L. A. Hillenbrand & J. M. Carpenter 2000; P. W. Lucas & P. F. Roche 2000; A. A. Muench et al. 2002; P. W. Lucas et al. 2005; M. Robberto et al. 2010; N. Da Rio et al. 2012; H. Drass et al. 2016; S. Meingast et al. 2016) and HST (K. L. Luhman et al. 2000; M. Andersen et al. 2011; M. Gennaro & M. Robberto 2020;

---

[10] Royal Society Dorothy Hodgkin Fellow.

M. Robberto et al. 2020). A small fraction of the candidates have been observed with ground-based spectroscopy to confirm their youth and late spectral types (L. A. Hillenbrand 1997; P. W. Lucas et al. 2001; C. L. Slesnick et al. 2004; P. W. Lucas et al. 2006; F. C. Riddick et al. 2007; D. J. Weights et al. 2009; L. A. Hillenbrand et al. 2013; P. Ingraham et al. 2014). Given its unmatched infrared (IR) sensitivity and wide array of camera filters, the James Webb Space Telescope (JWST, J. P. Gardner et al. 2023) can identify brown dwarfs in the ONC more reliably and at lower masses than previous facilities. In particular, its high angular resolution greatly facilitates the detection of faint sources within the bright, spatially variable emission from the Orion Nebula (M. J. McCaughrean & S. G. Pearson 2023). In addition, the Near-Infrared Spectrograph (NIRSpec; P. Jakobsen et al. 2022) on JWST has a multiobject mode that can observe >10 ONC members simultaneously with the optimal sensitivity of slit spectroscopy (P. Ferruit et al. 2022). To demonstrate this capability, we have performed NIRSpec observations of a sample of brown dwarf candidates in the ONC that were selected from HST images (M. Robberto et al. 2020). This paper presents those data, which include proplyds near and below the hydrogen burning limit and a candidate for a protostellar brown dwarf.

2. Spectroscopy

2.1. NIRSpec Observations

We pursued spectroscopy of brown dwarf candidates in the ONC with NIRSpec on JWST through the guaranteed time observation program 1228 (PI: C. Alves de Oliveira). The observations utilized NIRSpec's microshutter assembly (MSA), which consists of four quadrants that each contain 365×171 shutters. The angular size of an individual shutter is $0\rlap{.}''2 \times 0\rlap{.}''46$. The MSA spans a field with a size of $3\rlap{.}'6 \times 3\rlap{.}'4$. The data are collected by two 2048×2048 detector arrays that have pixel sizes of $0\rlap{.}''103 \times 0\rlap{.}''105$. We selected the PRISM disperser for the ONC observations because it provides the best sensitivity and the widest wavelength coverage (0.6–5.3 μm) among the available options. The spectral resolution for PRISM data ranges from $\sim$40 to 300 from shorter to longer wavelengths.

The targets for NIRSpec were selected from near-IR images obtained with the Wide Field Camera 3 on HST (WFC3, R. A. Kimble et al. 2008) in 2015 through Treasury program 13826 (PI: M. Robberto). These images were taken in a filter that coincides with absorption bands of H_2O and CH_4 that are strong in brown dwarfs (J. D. Kirkpatrick 2005) and a filter that measures the neighboring continuum, corresponding to F139M and F130N, respectively. Measurements of astrometry and photometry for sources detected in the WFC3 images are available from M. Robberto et al. (2020), but we utilized a reduction of the data that we performed in 2017 during the initial preparations for the NIRSpec observations. We considered only the WFC3 images that are within a radius of $\sim$4′ from the center of the ONC.

In Figure 1, we have plotted a diagram of m_{130} versus $m_{130} - m_{139}$ for the WFC3 sources that are within the $5' \times 5'$ field near the center of the ONC that is shown in Figure 2. At progressively fainter magnitudes, members of the ONC are expected to have lower temperatures and increasing absorption in the bands overlapping with F139M, leading to bluer values of $m_{130} - m_{139}$ (M. Robberto et al. 2020). As a result, the bluest
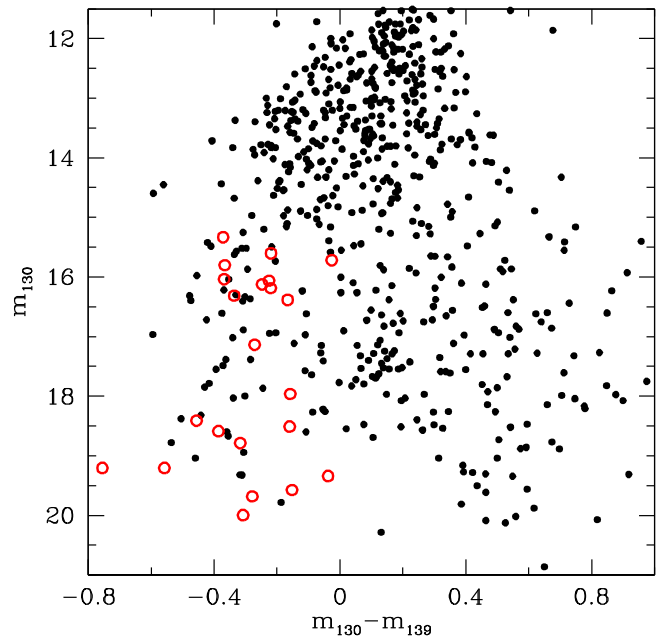

Figure 1. Color–magnitude diagram for sources within the field shown in Figure 2 based on images from HST/WFC3 (M. Robberto et al. 2020). We have obtained JWST/NIRSpec data for a sample of brown dwarf candidates that have $m_{130} - m_{139} < 0$ and $m_{139} > 15$ (circles).

sources at fainter magnitudes are the most promising candidates for substellar members of the ONC. Faint sources with redder colors should be a mixture of highly reddened brown dwarfs, stellar members that are seen in scattered light (edge-on disks and protostars), and background objects. The number of sources quickly increases with redder colors beyond $m_{130} - m_{139} \sim 0$, which likely reflects contamination from background stars and galaxies (M. Robberto et al. 2020), so we selected sources that have $m_{130} - m_{139} < 0$ for our sample of potential NIRSpec targets. We also required $m_{130} > 15$ to avoid saturation in NIRSpec. Among those with $m_{130} - m_{139} < -0.15$, higher priorities were assigned at fainter magnitudes. The candidates at $-0.15 < m_{130} - m_{139} < 0$ served as filler targets, which had the lowest priority.

We used the MSA Planning Tool (MPT) in the Astronomer's Proposal Tool (APT) to design two MSA configurations for observing a subset of the brown dwarf candidates identified with WFC3. We selected settings in MPT such that each target would be observed in three adjacent shutters that are equivalent to a single $0\rlap{.}''2 \times 1\rlap{.}''5$ slitlet, and each target would have a separation of $\geqslant 0\rlap{.}''059$ from the edges of the shutter. We required that the two MSA configurations have a separation less than the visit splitting distance (65″) so that they could be observed in a single visit. We used MPT to search for a pair of configurations that would (1) maximize the number of targets, particularly those at higher priorities, (2) avoid overlap of the MSA with the Trapezium stars since the shutters are not completely opaque, and (3) have suitable target acquisition stars (no close neighbors, not located in the brightest nebular emission, appropriate magnitudes). The targets for the selected MSA configurations are located north of the Trapezium stars. In Figure 2, we show 1.4–2.1 μm images for a field surrounding the MSA configurations obtained with NIRCam on JWST (M. J. Rieke et al. 2005, 2023) by M. J. McCaughrean & S. G. Pearson (2023). We have marked the field of view of the MSA for each pointing. Although we avoided the
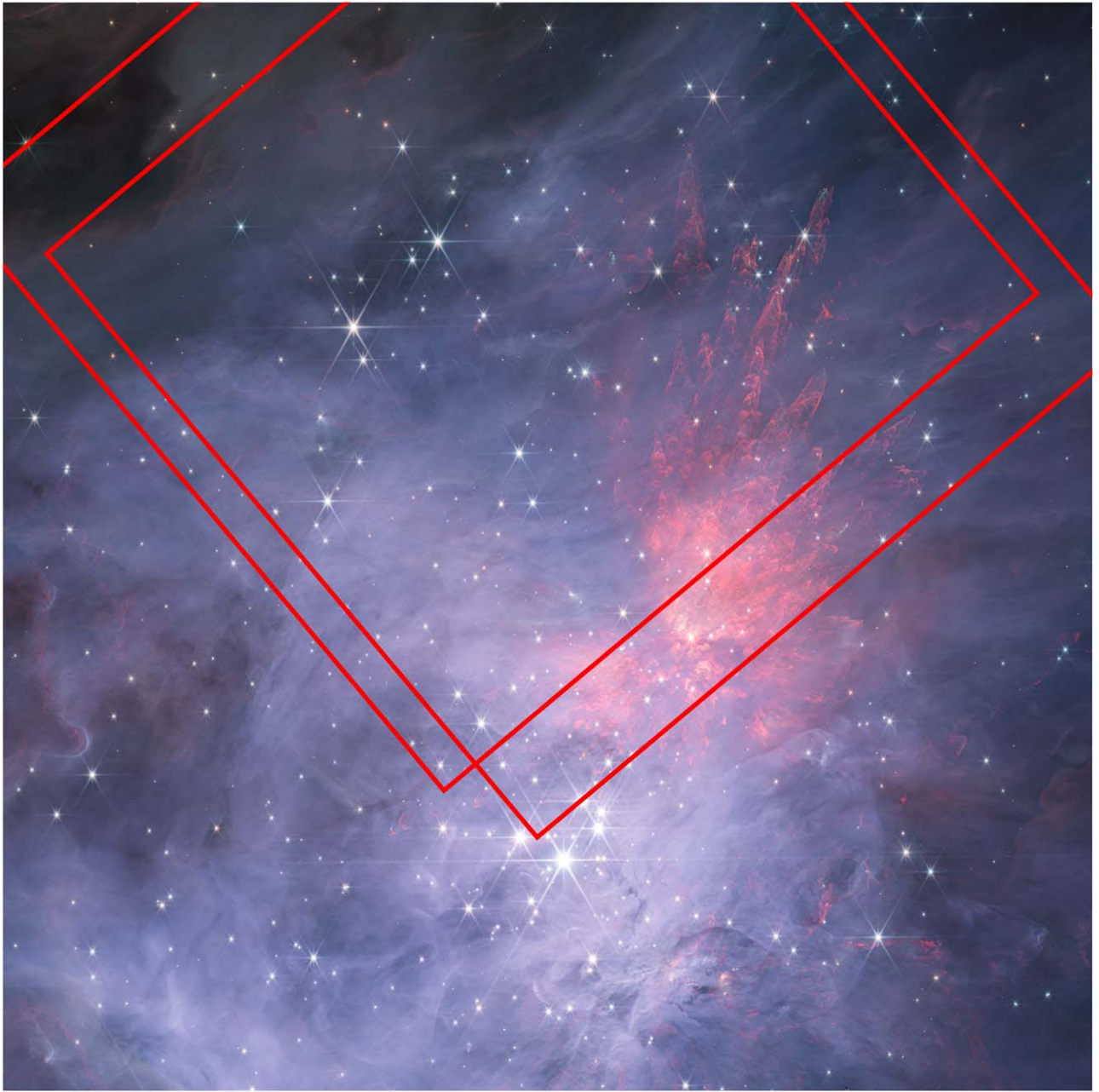
Figure 2. JWST/NIRCam images in five filters (F140M, F162M, F182M, F187N, F212N) for a $5' \times 5'$ field in the center of the ONC (M. J. McCaughrean & S. G. Pearson 2023). We have indicated the field of view for the NIRSpec MSA at two pointings (rectangles). The fluxes are displayed on a logarithmic scale. North is up and east is left.

Trapezium stars, one of the MSA configurations did overlap with the Becklin–Neugebauer (BN) object (E. E. Becklin & G. Neugebauer 1967), which is faint in WFC3 bands but is very red and becomes extremely bright longward of 2 μm. It is the bright source at the center of the red nebula in Figure 2. Enough light from BN leaked through the closed shutters of the MSA to contaminate the data for two targets (Section 2.2).

A total of 14 targets were observed in each of the two MSA configurations. Three sources were present in both configurations, so the total number of targets was 25. The NIRSpec data for three targets were not useful (Section 2.2). The remaining 22 sources are listed in Table 1, which includes the source numbers from the MPT catalog, equatorial coordinates measured from the NIRCam images, spectral types, and

extinction estimates. One of the targets, source 143 ([OW94] 130−119), was previously classified as a Herbig–Haro (HH) object (J.-K. Lee & M. G. Burton 2000), and thus should have been omitted from our sample of brown dwarf candidates. Four of the targets had filler status during the design of the MSA observations. NIRSpec reveals one to be a proplyd near the hydrogen burning limit (source 69, Section 3.2) and the other to be a brown dwarf that may be protostellar (source 126, Section 3.4).

The observations with the two MSA configurations were performed on 2023 February 22 (UT). At each of the three nod positions, one exposure was taken, which utilized five groups, six integrations, and the NRSRAPID readout pattern. The latter was chosen to avoid saturation for the brightest targets. In a

Table 1
Sources in the ONC Observed with NIRSpec

ID[a]	Other Name	α (ICRS) (deg)	δ (ICRS) (deg)	Spectral Type[b]	A_K (mag)	IR Excess?
120	⋯	83.783557	−5.354912	M6.5	0.03	no
69	[OW94] 181−247	83.825379	−5.379750	M6.5	0.43	yes
87	⋯	83.819875	−5.369885	M7	1.6	yes
118	⋯	83.802672	−5.346444	M7.25	0.62	no
67	⋯	83.831989	−5.376165	M7.25	0.32	?
117	[OW94] 131−046	83.804451	−5.346074	M7.5	0.21	?
129	⋯	83.814513	−5.328743	M8	0.11	no
80	⋯	83.823234	−5.374392	M8	0.27	no
123	⋯	83.824008	−5.324508	M8	0.50	no
113	⋯	83.800496	−5.352120	M8	0.48	no
139	⋯	83.847259	−5.346673	M8	1.1	no
126	⋯	83.815390	−5.330094	M8	1.6	yes
94	⋯	83.836852	−5.353779	M8.25	0.55	no
85	IRc8	83.811316	−5.376508	M8.5	0.17	?
90	⋯	83.826230	−5.363722	M8.5	0.24	?
96	⋯	83.825203	−5.361406	M8.75	0.19	no
95	⋯	83.823873	−5.362438	M9–L2	0.11	no?
133	⋯	83.789722	−5.334200	M9–L2	0.10	no?
109	⋯	83.814127	−5.346510	M9–L2	0.10	no?
127	⋯	83.821114	−5.326022	M9–L4	0.19	no?
142	⋯	83.799902	−5.325853	M9–L4	0.19	no?
143	[OW94] 130−119	83.804169	−5.355232	⋯	⋯	⋯

Notes.
[a] Source numbers that we assigned in the MPT/APT catalog for JWST program 1228.
[b] Uncertainties are 0.5 subclass unless indicated otherwise.

given MSA configuration, the total exposure time for three exposures was 1160 s. The charged time was 2.58 hr.

2.2. Data Reduction

To reduce the NIRSpec data, we began by retrieving the uncal files from the Mikulski Archive for Space Telescopes (MAST): doi:10.17909/zj8z-bs59. Those files were processed in the manner described by K. L. Luhman et al. (2024) for NIRSpec observations in IC 348. That study utilized a custom version of the pipeline developed by the ESA NIRSpec Science Operations Team (P. Ferruit et al. 2022) and based on the workflow and algorithms described in C. Alves de Oliveira et al. (2018).

Since the NIRSpec data were collected at three nod positions in each MSA configuration, the background subtraction for a given nod can utilize the average of the other two nods or only one of them. The average was our default choice, but for a few nods, we omitted one of the other nods in the background subtraction because of the presence of a second source or artifact in the slit or a variation in the background emission along the slit. For five sources (80, 85, 95, 113, 143), one of the nods was not used because neither of the other two nods produced adequate background subtraction. After subtraction, some of the nods exhibited small positive or negative residuals at the wavelengths of nebular emission lines, which are likely caused by spatial variations in the background emission. We interpolated the continua of the spectra across these residuals. The weaker emission lines that remain in the spectra may arise from either the sources or the nebula. For a few objects, all of the nods contained strong emission lines with similar strengths, indicating that the lines are concentrated on those objects. We have ignored the data for source 85 longward of 3 μm because of contamination by light from BN leaking through the MSA.

For three sources, the wavelength ranges falling on the detectors were too limited to be useful, so we do not report their spectra. One of those objects was also affected by artifacts related to BN. The reduced NIRSpec data for the remaining 22 targets are presented in Figures 3–5. The signal-to-noise ratios are >50 for most wavelengths and objects. The spectrum of source 113 has a negative residual near 3.3 μm that corresponds to the brightest emission feature from polycyclic aromatic hydrocarbons and reflects imperfect background subtraction.

2.3. Spectral Classifications

Source 143 ([OW94] 130−119) was identified as an HH object based on narrowband imaging in transitions of H_2 and [Fe II] (J.-K. Lee & M. G. Burton 2000). Its NIRSpec spectrum is dominated by emission in H I, H_2, and the fundamental band of CO. Previous studies of broadband mid-IR images have suggested that some HH objects produce bright CO emission (M. Takami et al. 2010; A. Tappe et al. 2012), which was recently confirmed with NIRSpec (T. P. Ray et al. 2023). Our data for source 143 provide additional evidence of that kind.

The remaining NIRSpec targets exhibit (1) strong H_2O absorption bands that indicate spectral types of late M through L and (2) gravity-sensitive features that indicate young ages, which include the triangular shape of the H-band continuum (P. W. Lucas et al. 2001) and the weak CO band at 4.4–5.2 μm (K. L. Luhman et al. 2023). The youth of the targets supports their membership in the ONC.

We have estimated spectral types and reddenings through visual comparison of the NIRSpec data at <2.5 μm to standard spectra for young stars and brown dwarfs (M0–L7, K. L. Luhman et al. 2017). For each spectral type in the range of the standards, progressively larger reddening (E. F. Schlafly et al. 2016) was
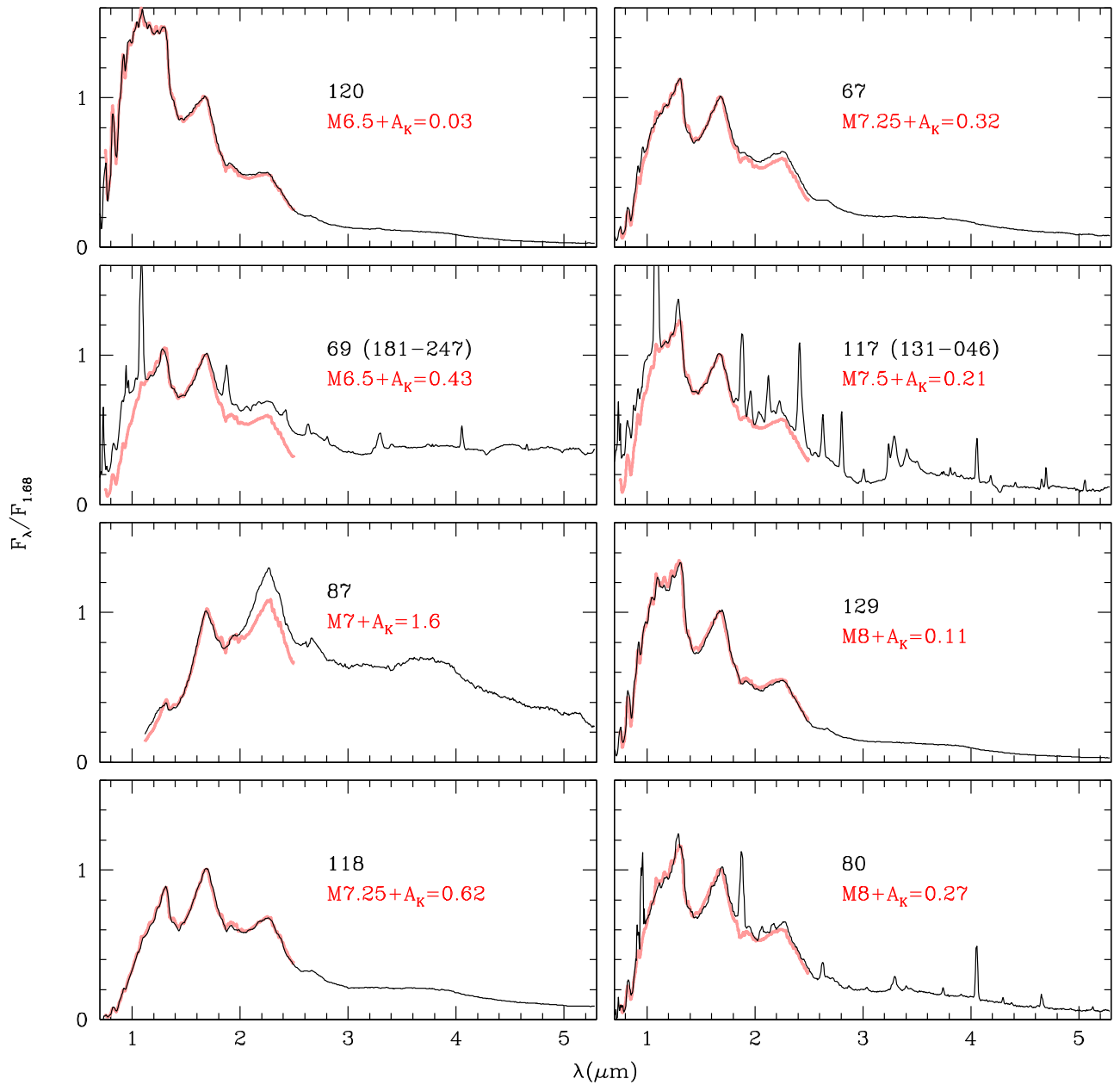
Figure 3. JWST/NIRSpec spectra of brown dwarf candidates in the ONC. The spectra are labeled with the source numbers from Table 1 and are compared to young standard spectra that have been reddened to match the slopes from 1.2 to 1.7 μm (K. L. Luhman et al. 2017).
(The data used to create this figure are available in the online article.)

applied to the standard until it matched the slope of a given NIRSpec target. From among those reddened standards, we then identified the spectral type that provided the best match to the absorption features. The resulting types range from M6.5 to early L. In Figures 3–5, we show the NIRSpec data in order of spectral type. Each spectrum is compared to a standard for the best matching spectral type and reddening. The standards are reddened to match the ONC objects at 1.2–1.7 μm, which usually produces good matches to the entire slopes at <2.5 μm. A few objects (69, 87, 126) have large excesses in the K-band relative to the standards. They also show excesses at longer wavelengths relative to the bluest (photospheric) sources at similar spectral types (Section 3.3), indicating the presence of increasing emission at longer wavelengths from circumstellar dust. For the

sources with K-band excesses, nonnegligible disk emission could extend to shorter wavelengths and weaken the H_2O band at 1.4 μm, resulting in spectral type estimates that are slightly too early. The coolest objects are consistent with wider ranges of spectral types (e.g., reddened late M to unreddened L), reflecting degeneracies between spectral type and reddening in low-resolution near-IR spectra of young L dwarfs (K. L. Luhman et al. 2017).

Source 113 is one of our faintest targets, but it is not among the coolest according to our classification (M8). As a result, it is unusually faint for its spectral type among members of the ONC. Similarly, it appears underluminous in color–magnitude diagrams constructed from NIRCam photometry for the cluster. This characteristic of source 113 may indicate that it is observed primarily in scattered light. Many underluminous
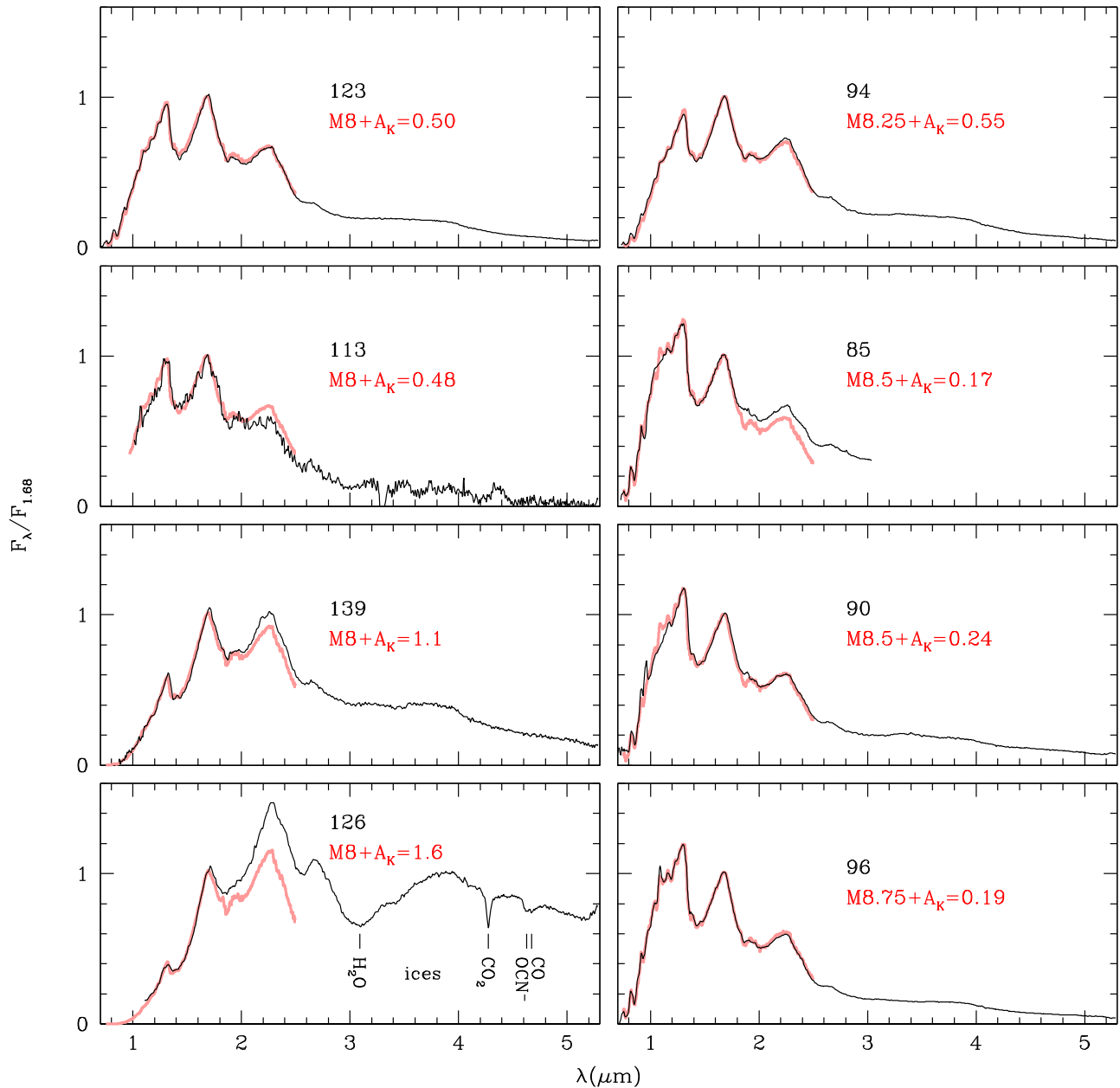
Figure 4. More JWST/NIRSpec spectra in the ONC.

sources have been previously found during spectroscopy of brown dwarf candidates in the ONC (C. L. Slesnick et al. 2004).

Previous studies have reported spectral types for two of our targets, sources 96 (M7.5 ± 1.5, C. L. Slesnick et al. 2004) and 120 (M3.75–M5, P. Ingraham et al. 2014). Our classifications are M8.75 and M6.5, respectively. Source 120 is 1.″7 from a brighter and earlier star, which may have contaminated the previous ground-based spectrum.

It is useful to consider the ONC sources in the context of the coolest young brown dwarfs that have been observed spectroscopically with NIRSpec. None of our targets are as cool as the L-type companion TWA 27B (G. Chauvin et al. 2004) based on comparisons to its NIRSpec data (K. L. Luhman et al. 2023). NIRSpec has recently discovered absorption features from an unidentified aliphatic hydrocarbon in two members of IC 348 (K. L. Luhman et al. 2024). These features are not

detected in any of the ONC targets, which is not surprising since their photometry would suggest that they probably do not extend down to the masses and temperatures of the objects in IC 348.

3. Properties of Brown Dwarfs

3.1. Mass Estimates

The earliest spectral type among the NIRSpec targets is M6.5, which should correspond to a mass near the hydrogen burning limit based on temperature scales for young stars (K. L. Luhman et al. 2003) and theoretical evolutionary models (I. Baraffe et al. 1998, 2015; G. Chabrier et al. 2023). The extinction-corrected magnitudes of the targets are as faint as $m_{130} \sim 19.6$. For that limit, the models from G. Chabrier et al. (2023) suggest masses of 0.003–0.007 $M_\odot$ assuming an age
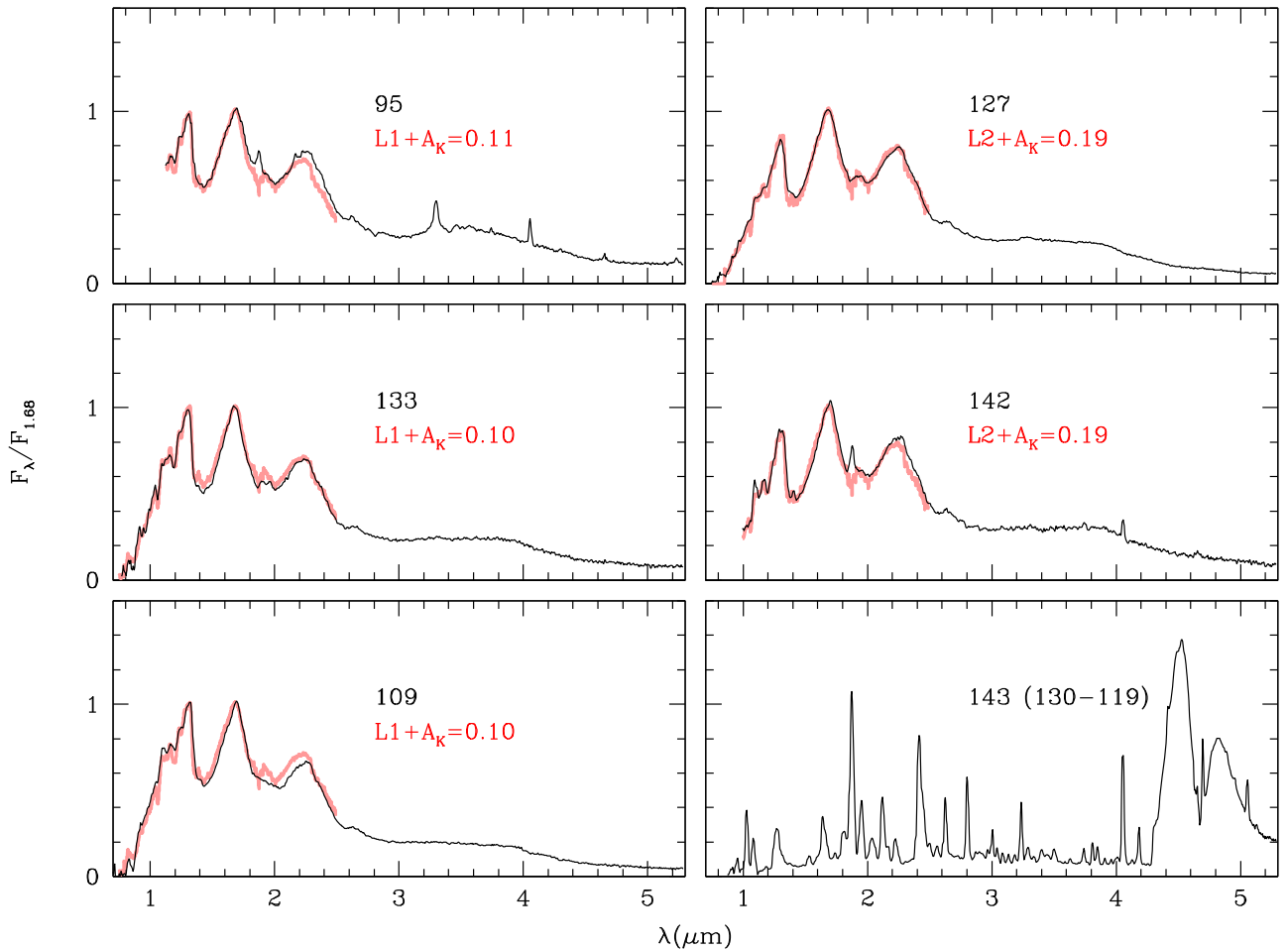
Figure 5. More JWST/NIRSpec spectra in the ONC.

range of 1–5 Myr for members of the ONC (R. D. Jeffries et al. 2011).

3.2. Proplyds

Two of the NIRSpec targets, source 69 ([OW94] 181−247) and source 117 ([OW94] 131−046), have been previously identified as proplyds based on optical images from HST (C. R. O'Dell & S. K. Wong 1996). Those data included filters that measure emission lines of H I, N II, and O III, which trace the ionization front in a proplyd. Each object exhibits a tear-drop-shaped nebula with a tail that points away from θ^1 C Ori. Dust continuum emission at millimeter wavelengths combined with a standard gas-to-dust ratio implies disk masses of 6.2 ± 1.0 and $2.2 \pm 0.4\,M_{\rm Jup}$ for sources 69 and 117, respectively (J. A. Eisner et al. 2016).

As expected, the NIRSpec data for the two proplyds contain strong emission lines, most notably from H I and He I (Figure 3). In addition, the spectra exhibit absorption bands from H_2O that indicate late spectral types. In Section 2.3, we estimated types of M6.5 and M7.5 for sources 69 and 117, respectively. It is difficult to estimate masses of central stars in proplyds from photometry because of reddening, line emission, and scattered light, but these spectral types should correspond to masses near and below the hydrogen burning limit (Section 3.1). Source 69 appears to have K-band excess emission relative to young standard spectra (Figure 3), so its

true spectral type could be slightly later than our estimate (Section 2.3).

Since the discovery of sources 69 and 117, additional high-resolution images have been taken with the Advanced Camera for Surveys (ACS) on HST (L. Ricci et al. 2008; M. Robberto et al. 2013) and NIRCam on JWST (M. J. McCaughrean & S. G. Pearson 2023). In Figure 6, we show images for a selection of the available filters that illustrate the colors of the central sources and that detect the ionization fronts, consisting of three broadband filters (F435W, F775W, F115W) and two narrowband filters that measure Hα+[N II] (F658N) and Paschen α (F187N). Each of the central sources is absent in F435W and F658N and is detected in the remaining bands, becoming brighter at longer wavelengths, which reflects a combination of late spectral types and extinction (Figure 3). For source 69, the area within the ionization front is darker in F435W and F658N than the background emission that surrounds the proplyd, which we interpret as a silhouette of the disk. As the flux of the central source increases at longer wavelengths, its point-spread function makes it more difficult to detect a silhouette, but one may be present in F187N as well. The radius of the silhouette is $\sim 0\rlap{.}''08$, corresponding to ~ 30 au at the distance of the ONC. Source 117 may also contain a smaller silhouette disk in F435W and F658N.

One additional NIRSpec target, source 80, has strong emission lines that are suggestive of a proplyd (Figure 3). It
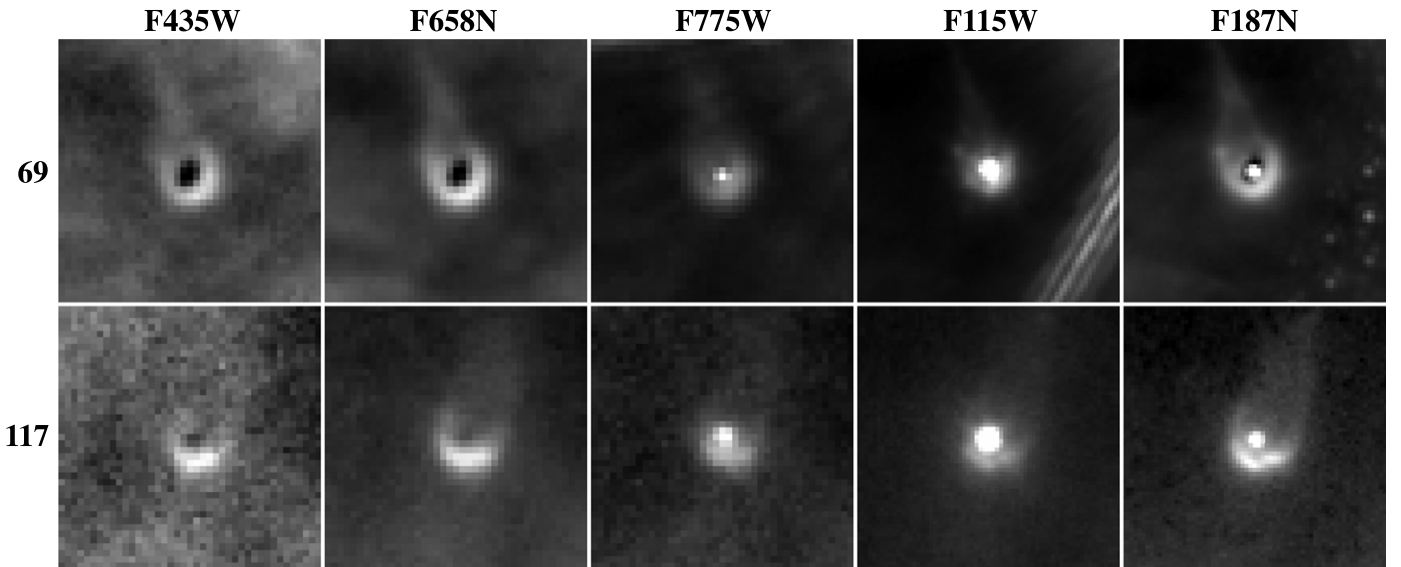
F435W	F658N	F775W	F115W	F187N

Figure 6. HST/ACS and JWST/NIRCam images of two ONC proplyds observed by NIRSpec (L. Ricci et al. 2008; M. Robberto et al. 2013; M. J. McCaughrean & S. G. Pearson 2023). The size of each image is $2'' \times 2''$. North is up and east is left.

is a point source in the available images from HST and JWST, so it may have an ionization front that is too small to resolve.

Two candidates for substellar proplyds have been highlighted in previous work, both of which are located in the ONC. One of the objects is [OW94] 124−132, which consists of a $0''15$ binary system that has a silhouette disk at shorter wavelengths and is surrounded by an ionization front (C. R. O'Dell & S. K. Wong 1996; N. Smith et al. 2005; M. Robberto et al. 2008). M. Robberto et al. (2008) proposed that the components of the binary are substellar based on their photometry. However, spectroscopy of the system is not available, and its relatively red color of $m_{130} - m_{139} = 0.14$ (M. Robberto et al. 2020) appears to be inconsistent with a late spectral type for its estimated extinction (M. Robberto et al. 2008). The second previous candidate for a brown dwarf proplyd is [OW94] 133−353 (C. R. O'Dell & S. K. Wong 1996; L. Ricci et al. 2008; M. Fang et al. 2016), which is one component of a $1''$ pair. In HST and JWST images, it appears as a point source with extended emission pointed away from θ^1 C Ori. The direction and cometary shape of the extended emission are suggestive of a proplyd. If an ionization front surrounds the central source, it is unresolved. M. Fang et al. (2016) performed spectroscopy on the object, measuring a spectral type of M9.5. Its $m_{130} - m_{139}$ color is also sufficiently blue to indicate a late spectral type (M. Robberto et al. 2020). With a magnitude of $m_{130} = 14.4$, it is unusually bright for its spectral type among members of the ONC.

Dozens of additional proplyds in the ONC are faint enough to be substellar (L. Ricci et al. 2008), but they also could be stars that are observed through high extinction or primarily in scattered light. Only a few of these objects have spectral classifications, which include [OW94] 179−354 and [OW94] 044−527 (J. Bally et al. 1998, 2000). The former has optical and IR types of K8–M3 and M7.5, respectively (C. L. Slesnick et al. 2004). New spectroscopy would be useful to resolve these discrepant types. The second source has been classified as M8.25–M8.5 (D. J. Weights et al. 2009; P. Ingraham et al. 2014), which should place it well below the hydrogen burning limit.

3.3. Excess Emission from Disks

The NIRSpec data extend to long enough wavelengths to potentially encompass emission from dust in circumstellar disks. Therefore, we can use these data to search for evidence of disks. The cool dust in a disk generates IR continuum emission that appears as an excess above that expected from the stellar photosphere. The size of the excess grows with longer wavelengths, causing the observed spectrum of the system to be redder than the photosphere alone. Our sample is large enough that it should contain both diskless and disk-bearing objects, so we have compared the spectral slopes among the targets to identify the two populations. For this analysis, the spectra are corrected for the extinctions derived during the spectral classifications and are normalized at 1.68 μm, as done for the observed spectra in Figures 3–5. In addition, the comparisons are performed for groups of objects with similar spectral types since photospheric spectral slopes vary with type. Near a given spectral type, most of the spectra have similar slopes, spanning a range of $\sim$0.1 mag at 3–5 μm when normalized at 1.68 μm, and a minority are significantly redder, which correspond to stellar photospheres and disk-bearing sources, respectively. In Table 1, we indicate whether we find excesses for each of the targets. Three objects have large IR excesses ($>$0.5 mag at 3–5 μm), consisting of sources 69, 87, and 126. A few additional sources may have small excesses ($\sim$0.2 mag), but data at longer wavelengths are needed for confirming the presence of disks. Their IR excess flags are listed as "?" in Table 1. As mentioned in Section 2.3, the cooler objects in our sample are consistent with wider ranges of types, so their extinctions and photospheric colors are uncertain, making it more difficult to reliably identify excesses from disks. We do not find large excesses for any of those objects, but smaller excesses are possible. Therefore, their IR excess flags appear as "no?" in Table 1. Disks around brown dwarfs often do not produce significant excesses at wavelengths shortward of 5 μm (K. L. Luhman et al. 2010), so the objects that lack large excesses in the NIRSpec data can still have disks, as in the case of one of the proplyds in our sample, source 117.

3.4. Candidate for Edge-on Disk or Protostar

One of the NIRSpec targets with IR excess emission, source 126, is distinctive in that it shows absorption bands near 3 and 4.27 μm and a blend of two bands centered near 4.62 and 4.67 μm (Figure 4). These features have been observed in edge-on disks and class I protostars and have been attributed to ices that contain H_2O, CO_2, OCN^-, and CO, respectively (W. F. Thi et al. 2002; Y. Aikawa et al. 2012; A. C. A. Boogert et al. 2022; J. Kim et al. 2022; J. A. Sturm et al. 2023; S. A. Federman et al. 2024). Given its high extinction ($A_K = 1.6$), the object could be either an edge-on class II system that is reddened by the molecular cloud or a class I protostar.[11] Measurements of the spectral energy distribution at IR wavelengths longward of the NIRSpec data are needed to distinguish between these two possibilities, but they are not available. To our knowledge, source 126 is the first object in any star-forming region that has been spectroscopically classified to be cool enough to be substellar, and that has detections of these ice features.

One edge-on disk has been previously detected around a brown dwarf (K. L. Luhman et al. 2007), which has silicate absorption at 10 μm from the occulting disk. It likely has the same ice features observed in source 126, but it has not been observed spectroscopically at those wavelengths. Meanwhile, a few dozen candidates for class 0 and I brown dwarfs have been identified (L. Hartmann et al. 1999; B. Riaz et al. 2017), primarily with the Spitzer Space Telescope (C. H. Young et al. 2004; T. L. Bourke et al. 2006; M. M. Dunham et al. 2008; D. Barrado et al. 2009). They appear to have luminosities low enough to be substellar based on their IR spectral energy distributions, but most lack the spectroscopy needed for confirmation of late spectral types. For the protostellar candidates that do have spectra, the spectral classifications have been indicative of stellar masses (K. L. Luhman & E. E. Mamajek 2010; K. L. Luhman & T. L. Esplin 2022). Source 126 appears to be the first candidate for a protostellar brown dwarf that has been shown to have a late spectral type.

4. Conclusions

We have used JWST/NIRSpec to perform multiobject spectroscopy of brown dwarf candidates in the ONC, which were selected from HST/WFC3 images (M. Robberto et al. 2020). Our results are summarized as follows:

1. We have observed 22 brown dwarf candidates near the center of the ONC with two MSA configurations of NIRSpec. Data were collected with the PRISM disperser, which provided a wavelength coverage of 0.6–5.3 μm and a resolution ranging from $\sim$40 to 300.
2. One of the targets, [OW94] 130−119, was previously classified as an HH object (J.-K. Lee & M. G. Burton 2000). Its NIRSpec spectrum exhibits strong emission in H I, H_2, and the fundamental band of CO. As with other recent NIRSpec observations (T. P. Ray et al. 2023), our data confirm that HH objects can produce bright emission in that CO band.
3. The remaining NIRSpec targets are cool and young based on strong H_2O absorption bands and gravity-sensitive features, as expected for substellar members of the ONC. We have estimated spectral types and extinctions from these data through comparison to young standard spectra. The resulting types range from M6.5 to early L. Based on theoretical evolutionary models (G. Chabrier et al. 2023), the earliest object should have a mass near the hydrogen burning limit, while the faintest and coolest objects have mass estimates of 0.003–0.007 $M_\odot$ for ages of 1–5 Myr.
4. Two of the NIRSpec targets are known proplyds based on images from HST (C. R. O'Dell & S. K. Wong 1996). We have classified them as M6.5 and M7.5 with NIRSpec, making them two of the coolest and least massive known proplyds. In optical images from HST (L. Ricci et al. 2008), the M6.5 proplyd appears to exhibit a silhouette disk that has a radius of $\sim$0.″08 ($\sim$30 au).
5. For three objects in our sample, the NIRSpec data are significantly redder than expected for reddened photospheres, indicating the presence of IR excess emission from disks. One of those sources also shows absorption bands at 3–5 μm from ices containing H_2O, CO_2, OCN^-, and CO, which have been previously observed in edge-on disks and protostars. Given its high extinction, it could be either an edge-on class II system that is reddened by the molecular cloud or a class I protostar. To our knowledge, it is the first object spectroscopically classified as a brown dwarf that has detections of these ice features. In addition, it appears to be the first candidate for a protostellar brown dwarf that has spectroscopy confirming its late spectral type.
6. Our study has demonstrated the ability of JWST/NIRSpec to perform multiobject spectroscopy on brown dwarf candidates within the bright extended emission of the Orion Nebula. Given that capability and the high yield of confirmed brown dwarfs in our sample, it should be feasible to obtain spectra of a large, representative sample of brown dwarfs in the ONC that extends down to masses of $\sim$1 M_{Jup}.

ORCID iDs

K. L. Luhman https://orcid.org/0000-0003-2822-2951
C. Alves de Oliveira https://orcid.org/0000-0003-2896-4138
I. Baraffe https://orcid.org/0000-0001-8365-5982
G. Chabrier https://orcid.org/0000-0002-8342-9149

---

[11] The stages of a young stellar object consist of classes 0 and I (protostar +disk+infalling envelope), class II (star+disk), and class III (star; C. J. Lada & B. A. Wilking 1984; C. J. Lada 1987; P. André et al. 1993; T. P. Greene et al. 1994).

E. Manjavacas ⬤ https://orcid.org/0000-0003-0192-6887
R. J. Parker ⬤ https://orcid.org/0000-0002-1474-7848
P. Tremblin ⬤ https://orcid.org/0000-0001-6172-3403

References

Aikawa, Y., Kamuro, D., Sakon, I., et al. 2012, A&A, 538, A57
Alves de Oliveira, C., Birkmann, S. M., Böker, T., et al. 2018, Proc. SPIE, 10704, 107040Q
Andersen, M., Meyer, M. R., Robberto, M., Bergeron, L. E., & Reid, N. 2011, A&A, 534, A10
André, P., Ward-Thompson, D., & Barsony, M. 1993, ApJ, 406, 122
Bally, J., O'Dell, C. R., & McCaughrean, M. J. 2000, AJ, 119, 2919
Bally, J., Sutherland, R. S., Devine, D., & Johnstone, D. 1998, AJ, 116, 293
Baraffe, I., Chabrier, G., Allard, F., & Hauschildt, P. H. 1998, A&A, 337, 403
Baraffe, I., Hormeier, D., Allard, F., & Chabrier, G. 2015, A&A, 577, 42
Barrado, D., Morales-Calderónm, M., Palau, A., et al. 2009, A&A, 508, 859
Becklin, E. E., & Neugebauer, G. 1967, ApJ, 147, 799
Boogert, A. C. A., Brewer, K., Brittain, A., & Emerson, K. S. 2022, ApJ, 941, 32
Bourke, T. L., Myers, P. C., Evans, N. J., II, et al. 2006, ApJL, 649, L37
Chabrier, G., Baraffe, I., Phillips, M., & Debras, F. 2023, A&A, 671, A119
Chauvin, G., Lagrange, A.-M., Dumas, C., et al. 2004, A&A, 425, L29
Daffern-Powell, E. C., Parker, R. J., & Quanz, S. P. 2022, MNRAS, 514, 920
Da Rio, N., Robberto, M., Hillenbrand, L. A., Henning, T., & Stassun, K. G. 2012, ApJ, 748, 14
Drass, H., Haas, M., Chini, R., et al. 2016, MNRAS, 461, 1734
Dunham, M. M., Crapsi, A., Evans, N. J., II, et al. 2008, ApJS, 179, 249
Eisner, J. A., Bally, J. M., Ginsburg, A., & Sheehan, P. D. 2016, ApJ, 826, 16
Fang, M., Kim, J. S., Pascucci, I., Apai, D., & Manara, C. F. 2016, ApJL, 833, L16
Federman, S. A., Megeath, S. T., Rubinstein, A. E., et al. 2024, ApJ, 966, 41
Ferruit, P., Jakobsen, P., Giardino, G., et al. 2022, A&A, 661, A81
Flammini Dotti, F., Kouwenhoven, M. B. N., Cai, M. X., & Spurzem, R. 2019, MNRAS, 489, 2280
Gardner, J. P., Mather, J. C., Abbott, R., et al. 2023, PASP, 135, 068001
Gennaro, M., & Robberto, M. 2020, ApJ, 896, 80
Greene, T. P., Wilking, B. A., André, P., Young, E. T., & Lada, C. 1994, ApJ, 434, 614
Hartmann, L., Calvet, N., Allen, L., Chen, H., & Jayawardhana, R. 1999, AJ, 118, 1784
Hillenbrand, L. A. 1997, AJ, 113, 1733
Hillenbrand, L. A., & Carpenter, J. M. 2000, ApJ, 540, 236
Hillenbrand, L. A., Hoffer, A. S., & Herczeg, G. J. 2013, AJ, 146, 85
Hurley, J. R., & Shara, M. M. 2002, ApJ, 565, 1251
Ingraham, P., Albert, L., Doyon, R., & Artigau, E. 2014, ApJ, 782, 8
Jakobsen, P., Ferruit, P., Alves de Oliveira, C., et al. 2022, A&A, 661, A80
Jeffries, R. D., Littlefair, S. P., Naylor, T., & Mayne, N. J. 2011, MNRAS, 418, 1948
Kim, J., Lee, J.-E., Jeong, W.-S., et al. 2022, ApJ, 935, 137
Kimble, R. A., MacKenty, J. W., O'Connell, R. W., & Townsend, J. A. 2008, Proc. SPIE, 7010, 43
Kirkpatrick, J. D. 2005, ARA&A, 43, 195
Lada, C. J. 1987, in IAU Symp. 115, Star Forming Regions, ed. M. Peimbert & J. Jugaku (Dordrecht: Reidel), 1
Lada, C. J., & Wilking, B. A. 1984, ApJ, 287, 610
Lee, J.-K., & Burton, M. G. 2000, MNRAS, 315, 11
Lucas, P. W., & Roche, P. F. 2000, MNRAS, 314, 858

Lucas, P. W., Roche, P. F., Allard, F., & Hauschildt, P. H. 2001, MNRAS, 326, 695
Lucas, P. W., Roche, P. F., & Tamura, M. 2005, MNRAS, 361, 211
Lucas, P. W., Weights, D. J., Roche, P. F., & Riddick, F. C. 2006, MNRAS, 373, L60
Luhman, K. L., Adame, L., D'Alessio, P., et al. 2007, ApJ, 666, 1219
Luhman, K. L., Allen, P. R., Espaillat, C., Hartmann, L., & Calvet, N. 2010, ApJS, 186, 111
Luhman, K. L., Alves de Oliveira, C., Baraffe, I., et al. 2024, AJ, 167, 19
Luhman, K. L., Briceño, C., Stauffer, J. R., et al. 2003, ApJ, 590, 348
Luhman, K. L., & Esplin, T. L. 2022, AJ, 163, 26
Luhman, K. L., & Mamajek, E. E. 2010, ApJL, 716, L120
Luhman, K. L., Mamajek, E. E., Shukla, S. J., & Loutrel, N. P. 2017, AJ, 153, 46
Luhman, K. L., Rieke, G. H., Young, E. T., et al. 2000, ApJ, 540, 1016
Luhman, K. L., Tremblin, P., Birkmann, S. M., et al. 2023, ApJL, 949, L36
Maíz Apellániz, J., Barbá, R. H., Fernández Aranda, R., et al. 2022, A&A, 657, A131
McCaughrean, M. J., & O'Dell, C. R. 1996, AJ, 111, 1977
McCaughrean, M. J., & Pearson, S. G. 2023, arXiv:2310.03552
McCaughrean, M. J., & Stauffer, J. R. 1994, AJ, 108, 1382
Meingast, S., Alves, J., Mardones, D., et al. 2016, A&A, 587, A153
Muench, A. A., Getman, K., Hillenbrand, L., & Preibisch, T. 2008, in Handbook of Star Forming Regions, Vol. 1, The Northern Sky, ASP Monograph Series 4, ed. B. Reipurth (San Francisco, CA: ASP), 483
Muench, A. A., Lada, E. A., Lada, C. J., & Alves, J. 2002, ApJ, 573, 366
O'Dell, C. R., Muench, A., Smith, N., & Zapata, L. 2008, in Handbook of Star Forming Regions, Vol. 1, The Northern Sky, ASP Monograph Series 4, ed. B. Reipurth (San Francisco, CA: ASP), 544
O'Dell, C. R., & Wen, Z. 1994, ApJ, 436, 194
O'Dell, C. R., Wen, Z., & Hu, X. 1993, ApJ, 410, 696
O'Dell, C. R., & Wong, S. K. 1996, AJ, 111, 846
Ray, T. P., McCaughrean, M. J., & Caratti o Garatti, A. 2023, Natur, 622, 48
Riaz, B., Briceño, C., Whelan, E. T., & Heathcote, S. 2017, ApJ, 844, 47
Ricci, L., Robberto, M., & Soderblom, D. R. 2008, AJ, 136, 2136
Riddick, F. C., Roche, P. F., & Lucas, P. W. 2007, MNRAS, 381, 1077
Rieke, M. J., Kelly, D. M., & Horner, S. 2005, Proc. SPIE, 5904, 590401
Rieke, M. J., Kelly, D. M., Misselt, K., et al. 2023, PASP, 135, 028001
Robberto, M., Gennaro, M., Giulia Ubeira Gabellini, M., et al. 2020, ApJ, 896, 79
Robberto, M., Ricci, L., Da Rio, N., & Soderblom, D. R. 2008, ApJ, 687, L83
Robberto, M., Soderblom, D. R., Bergeron, E., et al. 2013, ApJS, 207, 10
Robberto, M., Soderblom, D. R., Scandariato, G., et al. 2010, AJ, 139, 950
Schlafly, E. F., Meisner, A. M., Stutz, A. M., et al. 2016, ApJ, 821, 78
Simon, M., Close, L. M., & Beck, T. L. 1999, AJ, 117, 1375
Slesnick, C. L., Hillenbrand, L. A., & Carpenter, J. M. 2004, ApJ, 610, 1045
Smith, N., Bally, J., Licht, D., & Walawender, J. 2005, AJ, 129, 382
Smith, K. W., & Bonnell, I. A. 2001, MNRAS, 322, L1
Sturm, J. A., McClure, M. K., Beck, T. L., et al. 2023, A&A, 679, A138
Takami, M., Karr, J. L., Haegon, K., Chen, H.-H., & Lee, H.-T. 2010, ApJ, 720, 155
Tappe, A., Forbrich, J., Martín, S., Yuan, Y., & Lada, C. J. 2012, ApJ, 751, 9
Thi, W. F., Pontoppidan, K. M., van Dishoeck, E. F., Dartois, E., & d'Hendecourt, L. 2002, A&A, 394, L27
Weights, D. J., Lucas, P. W., Roche, P. F., Pinfield, D. J., & Riddick, F. 2009, MNRAS, 392, 817
Young, C. H., Jørgensen, J. K., Shirley, Y. L., et al. 2004, ApJS, 154, 396